
Align as Ideal: Cross-Modal Alignment Binding for Federated Medical Vision-Language Pre-training

Zitao Shuai

EECS Department
University of Michigan
Ann Arbor, MI 48105
ztshuai@umich.edu

Liyue Shen*

EECS Department
University of Michigan
Ann Arbor, MI 48105
liyues@umich.edu

Abstract

Vision-language pre-training (VLP) has arisen as an efficient scheme for multimodal representation learning, but it requires large-scale multimodal data for pre-training, making it an obstacle especially for medical applications. To overcome the data limitation, federated learning (FL) can be a promising strategy to scale up the dataset for medical VLP while protecting data privacy. However, client data are often heterogeneous in real-world scenarios, and we observe that local training on heterogeneous client data would distort the multimodal representation learning and lead to biased cross-modal alignment. To address this challenge, we propose a **Federated Align as Ideal** (FedAID) framework for federated VLP with robustness to data heterogeneity, to bind local clients with an ideal cross-modal alignment. Specifically, to reduce distortions on global-aggregated features while learning diverse semantics from client datasets during local training, we propose to bind the cross-modal aligned representation space learned by local models with an unbiased one via guidance-based regularization. Moreover, we employ a distribution-based min-max optimization to learn the unbiased cross-modal alignment at each communication turn of federated pre-training. The experiments on real-world datasets demonstrate our method successfully promotes efficient federated multimodal learning for medical VLP with data heterogeneity.

1 Introduction

Vision-language pre-training (VLP) learns efficient multimodal representations by extracting latent semantics from a large amount of image-text pairs, where the dataset scale largely impacts the performance of the learned model (Oquab et al., 2023). However, enlarging multimodal pre-training dataset is a non-trivial challenge especially for medical applications which is restricted by privacy issues of clinical and patient data Ladbury et al. (2023). To collect and utilize data across different institutes, recent work Lu et al. (2023a) has attempted to introduce federated learning into the medical VLP domain.

However, in real-world scenarios, datasets collected from different institutes are always heterogeneous, which is a long-standing practical challenge in federated learning Ghosh et al. (2019); Zhang et al. (2023a); Huang et al. (2022). For example, one hospital receives a high proportion of patients with pneumonia, while another hospital may undertake more patients with Edema, due to the variety of patient cohorts and geographics. While the data heterogeneity would essentially damage the performance of the federally trained model, current medical multi-modal pre-training methods haven't taken this vital factor into consideration, which encounters the deployment of medical VLP

*Corresponding author

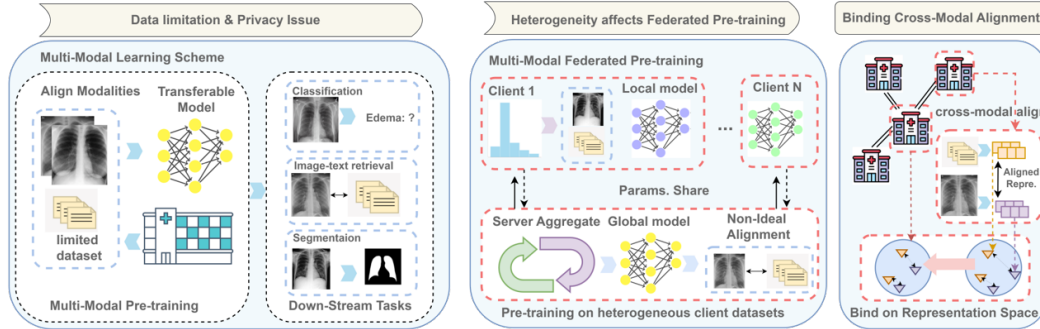


Figure 1: Federated multi-modal pre-training aims to decentralizedly utilize private datasets to tackle the data-hungry problem in pre-training transferable models. During local training, directly fitting heterogeneous local datasets that w.r.t. different distributions of latent semantics (e.g. disease) would result in non-ideal cross-modal alignment. Our method upgrades multi-modal pretraining methods to federated setting by binding local cross-modal alignment to an ideal one during local pre-training.

into decentralized pre-training scenarios. For a thorough study especially under the case of multi-modal learning, while multi-modal pre-training aims to learn a well-aligned latent space shared by each modality Zhang et al. (2022b); Li et al. (2021a), this cross-modal alignment would be affected by the data heterogeneity issue during local training Zhang et al. (2021); Ye et al. (2023), thus failing to provide an effective solution.

The current solution of simply averaging client models trained on heterogeneous local datasets is sub-optimal as shown in Fig. 1. First of all, when the client datasets are heterogeneous, re-training on the sent-back server model might distort the aggregated structure of the representation space. Secondly, as observed in empirical study Sec 5.2, averaging model parameters cannot produce an ideal alignment between two modalities which captures robust and factual diverse correlations between vision and language. And biased cross-modal alignment which overfits multi-modal correlations of local datasets, will not only affect generalization ability, but prevent the model from learning transferable and diverse semantics from local datasets. Furthermore, as we demonstrate in our empirical findings (Sec 5.2), heterogeneity harms the performance of pre-trained models by affecting the deep layers, which serve as alignment modules in the VLP model.

In this paper, we propose **Federated Align as IDEal (FedAID)** framework to mitigate data heterogeneity effect on encountering learning ideal cross-modal alignment in federated vision-language pre-training and enable its deployment in real-world scenarios. To alleviate the distortion on global-aggregated features during local client training while still encouraging models to extract diverse semantics from local datasets, we bind the cross-modal aligned representation space learned by local models to an unbiased representation space. Specifically, we introduce a teacher alignment module to provide robust cross-modal alignment by generating anchor representation space for regularization. We employ a distributionally robust optimization (DRO)-based algorithm to learn a robust teacher alignment module, which is optimized to better alleviate the worst-case distortion on the feature encoder caused by locally heterogeneous cross-modal alignment.

Our contributions primarily focus on:

- We for the first time tackle the problem of medical VLP under the federated setting by utilizing heterogeneous multi-modal datasets from different institutes. We conduct empirical studies to analyze the influence of data heterogeneity on federated multi-modal learning.
- We propose FedAID to mitigate the data heterogeneity on encountering learning ideal cross-modal alignment in federated VLP. Specifically, our method binds representations aligned by client models with unbiased representation space by introducing the guidance-based local training for learning unbiased cross-modal alignment to alleviate feature distortions.
- Experiment results show the effectiveness of our method in learning multi-modal representations under the federated setting by applying to various downstream tasks including image-text retrieval, classification, and segmentation.

2 Related Work

Medical Vision-Language Pre-training. Pre-training vision-language models on large-scale datasets and then transferring learned knowledge to downstream tasks has become a popular approach to leverage diverse semantics contained in multi-modal unlabeled data Li et al. (2022a); Bao et al. (2022); Radford et al. (2021). To obtain more generalizable representations, current works aim to learn the latent space shared by each modality using contrastive learning via cross-modal alignment Radford et al. (2021); Chen et al. (2020) or multi-modal fusion Li et al. (2021a); Chen et al. (2022), which connect the representations from the paired data. Existing works in medical vision-language model pre-training employ twin modality-specific encoders for mapping medical images and reports to the latent space respectively, and use the image-text contrastive loss Zhang et al. (2022b) to align visual and language representations. Improvement has been achieved by using the word-patch contrastive loss which aims to align fine-grained cross-modal representations Huang et al. (2021a). Furthermore, incorporating medical domain knowledge, Wang et al. (2022) proposes to align the image and report embeddings in three different granularities. Recent works have also tried to address other practical issues of misalignments Bannur et al. (2023). However, almost all of the current methods still rely on large-scale pre-training datasets, which impede the adoption to modalities with limited training samples and deployment in real-world scenarios.

Federated multi-modal learning. Federated multi-modal learning Zhou & Wang (2022) aims to facilitate diverse semantics in local datasets in a decentralized and privacy-preserved way. Related works often focus on leveraging client-side information to train personalized information while utilizing server-side pre-trained models. Su et al. (2022); Chen et al. (2023); Lu et al. (2023b), and use local datasets to enhance the centralized training Yu et al. (2023). However, these works haven't answered a key question: how can we decentralize the multi-modal pre-training through a federated way in real-world scenario to learn generalizable cross-modal representations? Recent advances Lu et al. (2023a) has verified that federated learning can be utilized to scale up the pre-training dataset. However, this work hasn't considered the harm of data heterogeneity issue Ghosh et al. (2019), which is very common and significant in practice such as in medical applications.

Heterogeneity in federated learning. Existing methods have tried to solve this problem in uni-modal supervised learning tasks Li & Wang (2019); Collins et al. (2021); Li et al. (2021b). These methods designed for supervised tasks focus on the heterogeneous problem in label distribution Diao et al. (2020) or feature distribution Li et al. (2022c), which cannot be directly adapted to the vision-language pre-training task. Recent works in representation-augmentation based uni-modal self-supervised federated learning Zhang et al. (2023a); Huang et al. (2022); Li et al. (2022b) employ additional communications on representations of local data to increase sample diversity. Such methods fail to protect data privacy, which is a vital concern in medical applications. Yan et al. (2023) utilizes image-side-only techniques to handle heterogeneity and thus may harm the learning of cross-modal alignment when adapted to the multi-modal setting. Zhuang et al. (2022); Li et al. (2021b) considers distillation-based methods yet ignores the direct modeling of cross-modal alignment. While the learned models can be biased and over-reliance on spurious correlations Saab et al. (2022) due to the data heterogeneity in the medical domain Krishnan et al. (2022), distributionally robust optimization Deng et al. (2020) can alleviate these issues by optimizing the group-wise worst-case performance on given objective Liu et al. (2022), thus can be flexibly adapted to various of federated learning tasks Han et al. (2023); Zhang et al. (2022a); Capitani et al. (2024).

3 Problem Formulation

We aim at mitigating the data heterogeneity issues in federally pre-training medical vision-language models from heterogeneous private client datasets. In this section, we will formulate the set-up of the Federated Vision-Language Pre-training task, which aims to capture generalizable cross-modal alignment by leveraging diverse semantics from local datasets. Then we will introduce our assumption on multi-modal pre-training data and heterogeneity. Please see Appendix F for detailed preliminary.

Federated Vision-Language Pre-training (FedVLP). We aim to federally pre-train medical vision-language models. Specifically, given N clients $\{C_i\}_{i=1}^N$, FedVLP decentralizedly conducts vision-language representation learning across clients, where local models are learned only on the local client dataset. The goal is to aggregate the locally trained models on a central server to obtain a generalizable and unbiased global pre-trained model. Here, we assume each client has a local yet

To federally leverage heterogeneous local datasets to pre-train an efficient vision-language model, we propose a decentralized framework that can robustly capture reliable cross-modal semantic alignments across different clients. As shown in Fig. 2, we employ the teacher alignment module to guide the local training, to learn factual diverse correlations between two modalities.

In this section, we first introduce our approach to reduce distortion on global-aggregated features during fitting local dataset via binding cross-modal alignments, through a guidance-based local training strategy. Secondly, we will illustrate our approach of employing the distributionally robust optimization to learn unbiased cross-modal alignment. Details can be seen in Algorithm 1.

4.1 Cross-Modal Alignment Binding via Guidance-Based Local Training

As shown in our empirical findings (Sec. 5.2), medical vision-language models pre-trained on heterogeneous client datasets are affected by the local correlations of the two modalities, which can't be addressed by simply averaging the weights of local models. Furthermore, this mainly falls on the deep layers which act as the cross-modal alignment module. As shown in Sec. A, we observe that a non-ideal alignment module would amplify bias in local datasets and enforce the encoder to learn biased features during local iterations and distort the global-aggregated features. Inspired by these findings, we design to separately handle the deep layers and shallow layers of the modality-specific network, which are considered to be the encoder and the alignment module, respectively. To encourage models to capture semantics in local datasets during local training, we keep updating the whole model during local training. To avoid feature distortion, we focus on the alignment module and bind the local cross-modal alignment to an ideal one.

Binding cross-modal alignments on the representation space. Binding local cross-modal alignments can be straightforwardly solved by replacing the local alignment module with a frozen unbiased one. *However, this is not practical due to our goal of encouraging models to learn semantics from local datasets. Besides, the unbiased alignment module of the current communication turn should also be updated.* To enable cross-modal alignment binding with fully learnable local models, we employ an alternative approach to minimize the distance between the representation space projected by local alignment modules and an anchor representation space.

As shown in Fig. 2, given input image-text pairs from dataset of client $c \in \mathcal{C}$ as $(x^c, y^c) \sim D_c$, where c is the index of client, the feature vectors output from the image and text encoder modules can be denoted as (I^c, T^c) , respectively. (I^c, T^c) will be aligned by alignment modules, and the aligned representations output from local aligners and anchor representations output from unbiased aligner are denoted by (z_I^c, z_T^c) , (z_I^{c*}, z_T^{c*}) respectively. During the local training, given the learning object of aligning two modalities $L_{task}(x, y)$ (e.g. image-text contrastive loss in ConVIRT Zhang et al. (2022b)), we have:

Remark 1 Consider L -lipschitz learning object $L_{task} : \mathbb{R}^{2d} \rightarrow \mathbb{R}, L_{task} > 0, d \in \mathbb{N}^+$. Minimizing $L_{task}(z_I^{c*}, z_T^{c*})$ can be reformulated as: $\min_{\theta} (L_{task}(z_I^c, z_T^c) + L (\|z_I^c - z_I^{c*}\|_2^2 + \|z_T^c - z_T^{c*}\|_2^2))$, where θ represents the model parameters. See detailed analysis in Appendix G.1.

Guiding local training with robust alignment module. To bind local cross-modal alignments, motivated by Remark 1, we can introduce a robust teacher alignment module to generate anchor representations conditioned on the output feature vector of the encoder, and leverage them for guiding local training. Specifically, given the local dataset of client $c \in \mathcal{C}$ sampled from $(x^c, y^c) \sim D_c$, and teacher alignment module g_I^*, g_T^* , we target at updating the feature encoders f_I, f_T and the corresponding alignment modules g_I, g_T , by training on the local client dataset D_c , under the guidance of teacher alignment modules. Following the above analysis, we aim to reduce the discrepancy between two sets of aligned representations produced by local and teacher alignment modules. Thus, given number N_c of samples in client c , the teacher guidance loss can be formulated as below:

$$\mathcal{L}_{guide} = \sum_{i=1}^{N_c} (z_{I,i}^* - z_{I,i})^2 + \sum_{i=1}^{N_c} (z_{T,i}^* - z_{T,i})^2. \quad (1)$$

We combine the guidance loss with the optimization goal \mathcal{L}_{task} of the initial medical vision-language pre-training method, which includes e.g. image-text contrastive loss in ConVIRT Zhang et al. (2022b). The overall loss function for guidance-based local client training can be written as:

$$\mathcal{L}_{local} = \mathcal{L}_{guide} + \alpha \mathcal{L}_{task} \quad (2)$$

where α is the hyper-parameter that balances between guidance regularization and training tasks.

4.2 Learning Unbiased Cross-modal Alignment via Distributionally Robust Optimization

As mentioned in section 4.1, we aim to utilize an anchor space to guide the local client training. To achieve this, we need to obtain a teacher alignment module that can capture globally unbiased and generalizable cross-domain alignment. How can we obtain such a teacher guidance model? We propose to learn such unbiased cross-modal alignment by considering the robustness across various distributions of local clients. Specifically, the teacher alignment module should encourage the model to learn well-aligned latent space while resulting in less feature distortion on the aggregated feature encoder during fitting local datasets. Furthermore, the robustness requires the teacher model to perform well on various data distributions. These insights motivate us to learn an alignment module that can well align representations and reduce feature discrepancy under various local clients, which would even well tackle the most severe distortion during local training. *This motivation inspires us to model the problem as a worst-case optimization problem, which can be solved by robust optimization (DRO) Cotter et al. (2019); Namkoong & Duchi (2016).* Detailed problem formulation and description can be seen in Appendix F.

Learning robust cross-modal alignment through distributionally robust optimization. Following the analysis above, we model the de-centralized pre-training framework as a two-stage DRO learning process. In the first stage, the whole model is jointly optimized with \mathcal{L}_{local} (Eq. 2), and the aggregated encoder f^* is obtained by server averaging. In the second stage, we employ the decentralized DRO to learn a robust teacher alignment module g^* that performs well conditioned on the worst-case local models and local data distribution where the feature encoder is distorted the most severely.

We employ an extra de-centralized learning process on the client side to optimize the alignment module on the worst-case distribution of an uncertainty set Namkoong & Duchi (2016) constructed by the local clients, with the distributions denoted as $P_i, i \in [1, \dots, N_c]$ for simplicity. The details of the uncertainty set can be seen in the Appendix Sec. F. Given teacher alignment module g^* and the aggregated encoder f^* , the optimization goal can be constructed based on the support distribution P_i in the uncertainty set:

$$\min_{g^*} \max_{\mathbf{w} \in \Delta_{N-1}} \sum_{i=1}^N w_i \mathcal{L}_{dro}(g^*, P_i, f^*), s.t. D(N\mathbf{w}|\mathbf{1}) \leq \rho \quad (3)$$

,where $\mathcal{L}_{dro}(g^*, P_i, f^*)$ is calculated on local clients. We will illustrate it in the following part.

Optimizing teacher alignment module via alternating min-max game. To match the newly learned semantics from local datasets during local training of each communication turn r , we aim to continually update the teacher alignment module. For each turn r , we employ an alternative optimization approach. We firstly complete the local training, and optimize \mathbf{w} via the mirror gradient descent process that could be solved efficiently Namkoong & Duchi (2016); Zhang et al. (2023b); Duchi et al. (2008):

$$w_i^{(r+1)} = \text{Proj}_{\mathcal{Q}_c} \left(w_i^{(r)} e^{\gamma v_i^{(r)}} / \sum_{i=1}^N w_i^{(r)} e^{\gamma v_i^{(r)}}, \rho \right) \quad (4)$$

where $\text{Proj}_{\mathcal{Q}_c}$ refers to the projection to $\{w : D(N\mathbf{w}|\mathbf{1}) \leq \rho\}$, v_i represents the loss $\mathcal{L}_{dro}(g^*, P_i, f^*)$. The weights \mathbf{w} will be used in updating g^* following Eq. 3 in local clients.

Finally, we propose the \mathcal{L}_{dro} to learn a g^* that can well align representations of the two modalities and reduce the discrepancy between anchor and local representations projected by g^* and local alignment module g during local training. To reduce the discrepancy, we directly minimize the distance of anchor and local representations modality-wise. Specifically, for client c , we use f^* to generate features (\tilde{I}, \tilde{T}) which are not distorted by the local aligner during the second stage’s training, and a learnable copy to generate distorted features (I, T) . (\tilde{I}, \tilde{T}) and (I, T) are input to g^* to get (z_I^*, z_T^*) and $(\tilde{z}_I^*, \tilde{z}_T^*)$ respectively. Then we minimize the L2 distance of them. To guarantee the alignment in latent space, we utilize multi-modal contrastive loss Radford et al. (2021); Zhang et al. (2022b) \mathcal{L}_{CL} between $(\tilde{z}_I^*, \tilde{z}_T^*)$ to guarantee to learn well-aligned latent space. To simulate the distortion by local training, we input (I, T) into g to get (z_I, z_T) to calculate \mathcal{L}_{task} . The learning object of the second stage of client c could be written as:

Algorithm 1 Cross-Modal Alignment Binding for Federated Pre-training

```

1: Input: Clients  $N$ ; Communication round  $R$ ; encoder  $\Theta^{(0)}$ ; align module
    $\theta^{(0)}$ ; robust align module  $\theta^{(0)*}$ ; client weight  $\{w_i^{(r)}\}_{i=1}^N = \frac{1}{N}$ ; uncertainty
   set radius  $\rho$ ; client datasets  $\{D_i\}_{i=1}^N$ ; Local iteration steps  $E$ .
2: for  $r = 0, \dots, R - 1$  do
3:   Server broadcasts  $\Theta^{(rE)}, \theta^{(rE)}, \theta^{(rE)*}, \{w_i^{(r)}\}_{i=1}^N$ 
4:   for client  $i = 1, \dots, N$  do
5:     Utilize Algorithm 2 on  $D_i$  to get  $\theta_i^{(r+1)E}, \Theta_i^{(r+1)E}$ 
6:   end for
7:   Server computes:  $\Theta^{(r+1)E} = \frac{1}{N} \sum_{i=1}^N \Theta_i^{(r+1)E}$ 
8:   for client  $i = 1, \dots, N$  do
9:     Compute loss  $v_i^{(r+1)}$  of model  $(\Theta_i^{(r+1)E}, \theta_i^{(r+1)E})$  on dataset  $D_i$ 
10:   end for
11:   for client  $i = 1, \dots, N$  do
12:      $w_i^{(r+1)} = \text{Proj}_{\mathcal{Q}_i} \left( w_i^{(r)} e^{\gamma v_i^{(r+1)}} / \sum_{i=1}^N w_i^{(r)} e^{\gamma v_i^{(r+1)}}, \rho \right)$ 
13:   end for
14:   for client  $i = 1, \dots, N$  do
15:     Utilize Algorithm 3 on  $D_i$  to get  $\theta_i^{(r+1)E*}$ 
16:   end for
17:   Server computes:  $\theta^{(r+1)E*} = \frac{1}{N} \sum_{i=1}^N \theta_i^{(r+1)E*}$ 
18:   Set parameters:  $\theta^{(r+1)E} = \theta^{(r+1)E*}$ 
19: end for
20: return  $(\Theta^{(RE)}, \theta^{(RE)})$ 

```

Algorithm 2 Guidance-Based Alignment Binding in Local Training

```

1: Input: client index  $i$ ; learning rate  $\eta$ ; weight update stepsize  $\gamma$ ; Local
   iteration steps  $E$ ; encoder  $\Theta^{(rE)}$ , local and teacher alignment module:
    $\theta^{(rE)}, \theta^{(rE)*}$ 
2: Set  $(\Theta_i^{(rE)}, \theta_i^{(rE)}, \theta_i^{(rE)*}) = (\Theta^{(rE)}, \theta^{(rE)}, \theta^{(rE)*})$ 
3: for  $t = rE, \dots, (r+1)E - 1$  do
4:   Sample  $\xi_i^{(t)}$  from  $D_i$  uniformly
5:    $(\Theta_i^{(t+1)}, \theta_i^{(t+1)}) = (\Theta_i^{(t)}, \theta_i^{(t)}) -$ 
6:      $\eta \nabla_{(\Theta_i, \theta_i)} \mathcal{L}_{\text{local}}((\Theta_i^{(t)}, \theta_i^{(t)}), \theta^{(rE)*}, \xi_i^{(t)})$ 
7: end for
8: The client sends  $\theta_i^{(r+1)E}, v_i^{(r)}$  to the server

```

Algorithm 3 Learning Robust Teacher Cross-Modal Alignment

```

1: Input: client index  $i$ ; learning rate  $\eta$ ; weight update stepsize  $\gamma$ ; Local
   iteration steps  $E$ ; encoder  $\Theta^{(r+1)E}$ , local and teacher alignment module:
    $\theta^{(r+1)E}, \theta^{(rE)*}$ ; client weight  $w_i$ 
2:  $(\Theta_i^{(r+1)E}, \theta_i^{(r+1)E}) = (\Theta^{(r+1)E}, \theta^{(r+1)E})$ 
3: Set  $\theta_i^{rE*} = \theta^{rE*}, \Theta_i^{rE*} = \Theta^{rE*}$ 
4: for  $t = rE, \dots, (r+1)E - 1$  do
5:   Sample  $\xi_i^{(t)}$  from  $D_i$  uniformly
6:    $(\theta_i^{(t+1)*}, \Theta_i^{(t+1)}) = (\theta_i^{(t)*}, \Theta_i^{(t)}) -$ 
7:      $w_i^{(r+1)} \eta \nabla_{\theta, \Theta} \mathcal{L}_{\text{dro}}(\Theta_i^{(t)}, \theta_i^{(t)}, \theta_i^{(t)*}, \Theta_i^{(t)*}, \xi_i^{(t)})$ 
8: end for

```

$$\mathcal{L}_{\text{dro}} = \beta \left(\sum_{i=1}^{N_C} (z_{T,i}^{\sim} - z_{T,i}^*)^2 \right) + \sum_{i=1}^{N_C} (z_{T,i}^{\sim} - z_{T,i}^*)^2 + \mathcal{L}_{CL} + \mathcal{L}_{\text{task}}. \quad (5)$$

5 Experiment

5.1 Experiment Setting

Pre-training setup. Following Wang et al. (2022), we utilize the MIMIC-CXR Bigolin Lanfredi et al. (2022) dataset for medical vision-language pre-training. During the de-centralized pre-training process, local clients only have access to their private datasets. Following Yan et al. (2023), we employ the Latent Dirichlet Allocation (LDA) Blei et al. (2003) to divide the MIMIC-CXR dataset based on a 5-way disease attribute to construct the heterogeneous client datasets. We set the heterogeneity degree in the LDA algorithm to be 1. The client datasets are highly heterogeneous as shown in Fig. 4 and the Appendix. We divide the MIMIC-CXR into 5 heterogeneous subgroups to construct 5 clients. Each divided dataset consists of train splits and test splits based on the notation of the MIMIC-CXR. For the pre-training reported in the main table, we set the number of communications to 25, and we randomly sampled 50 batches of data from the client datasets for each communication. For more details, please see the Appendix B.1.

Downstream tasks. We conduct several downstream tasks following Wang et al. (2022) to evaluate the generalization ability of the pre-trained model. For more details, please see the Appendix B.2. **(1). Few-shot classification.** We test their performance on multiple image classification benchmarks: (a). RSNA Pneumonia Detection (RSNA) Shih et al. (2019). (b) Covidx Wang et al. (2020). We fine-tune our pre-trained model with an additional linear layer on 1%, 10% percentage of the training dataset, and evaluate the classification accuracy. **(2). Medical image segmentation.** We conduct experiments following Wang et al. (2022) on medical image segmentation on the RSNA Wang et al. (2020) benchmark. We freeze the encoder and fine-tune a U-Net decoder using 1%, 10% of the training data, and then use the Dice score for evaluation. **(3). Image retrieval.** To verify the pre-trained models have learned semantics and cross-modal alignments, we conduct the image retrieval task. Specifically, we utilize the validation splits of the clients for evaluation, these datasets are unseen in pre-training. We utilize the top-1 recall accuracy and top-5 recall accuracy to evaluate the pre-trained models.

Backbones and Baselines. We focus on enabling medical vision-language pre-training (VLP) methods to be applied to heterogeneous federated learning scenes and have considered the generalization ability of FedAID on different backbone VLP methods. Since federated heterogeneous VLP is a new topic, we adopt existing medical VLP baselines to federated strategies Lu et al. (2023a). Specifically, we consider adopting contrastive learning based methods: simple language-image contrastive alignment (ConVIRT) Zhang et al. (2022b); Radford et al. (2021), global-local language-image contrastive alignment (GLoRIA) Huang et al. (2021a), and Multi-Granularity Cross-modal Alignment (MGCA) Wang et al. (2022). Since the federated multi-modal per-training is a novel setting, we adapted FedMAE Yan et al. (2023), FedEMA Zhuang et al. (2022), FedMOON Li et al. (2021b) for comparison. These are self-supervised learning methods in the federated learning domain which also

focus on tackling the data heterogeneity. For basic federated learning baselines, we consider simple averaging (FedAvg) McMahan et al. (2017); Lu et al. (2023a), decentralized training (Local), and centralized training (Global). For fair comparisons, we combine each federated learning strategy with different medical VLP methods. For baselines pre-trained in Local strategy, we report the averaged performance of the local models.

For fair comparisons, we re-implement the methods with the same backbones. To enable uni-modal self-supervised learning baselines to be applied to our setting, we employ the image-text contrastive loss with the same hyperparameters to our method for fairness. We utilize a ViT-base Dosovitskiy et al. (2020) as our vision encoder and utilize the Bert-base Devlin et al. (2018) as our text encoder. We pre-process the input following Wang et al. (2022). We utilize an additional transformer layer from ViT-base and Bert-base as the align module for vision and language respectively.

5.2 Empirical Finding

In this section, we will demonstrate our key empirical findings for federated multi-modal pre-training under heterogeneous client datasets, which actually motivates us to propose our Federated distributional Robust Guidance-Based (FedAID). We conduct experiments on the image-text retrieval task, which reflects the ability to capture vision-language alignments. Due to the page limitation, here we list our key findings, detailed results can be seen in the Appendix A:

- FedAvg can aggregate semantics from local clients, but the performance would be damaged by data heterogeneity as shown in Fig. 5.
- Fig. 6 shows retraining server model on local datasets would distort its feature encoders.
- Fig. 7 shows diverse info. is aggregated in shallow layers that extract feature semantics.
- De-centralized pre-trained deep layers that act as the align module is harmful for extracting diverse semantics as shown in Fig. 8.

Overall, from empirical findings, we conclude that federated multimodal pre-training is sensitive to data heterogeneity which results in learning distorted cross-modal alignment. Simply averaging local model weights does not solve this issue essentially. Thus, we are motivated to propose our method.

Table 1: Downstream task performance. We report the few-shot classification accuracy on Covid and RSNA, the retrieval accuracy on Chest imaGenome, and the Dice score for segmentation on RSNA.

Strategy	RSNA (cls.)		Covid (cls.)		RSNA (seg.)		Chest imaG. (ret.)			
	1%	10%	1%	10%	1%	10%	Rec.@1	Rec.@5	Wst.@1	Wst.@5
ImageNet Init ViT	79.02	80.62	63.75	83.75	60.09	67.02	3.64	16.46	2.86	14.17
FedMAE	80.81	81.06	77.50	85.75	69.48	73.38	8.29	33.03	6.92	30.49
FedEMA	82.81	83.19	79.25	86.50	70.94	73.65	24.01	67.05	21.85	62.44
FedMOON	82.51	83.21	77.75	89.25	68.99	71.28	27.85	70.88	25.34	67.19
FedAvg	83.19	83.31	78.00	88.50	69.59	71.50	28.83	72.12	25.34	66.68
FedAID (Ours)	83.21	83.54	82.50	90.00	71.51	74.08	29.49	73.03	26.99	67.65
Centralized	83.39	84.61	82.50	92.00	72.60	76.35	41.45	84.22	38.55	79.98

Table 2: Downstream task performance on different multi-modal pre-training backbone methods.

Strategy	Method	RSNA (cls.)		Covid (cls.)		RSNA (seg.)		Chest imaG. (ret.)			
		1%	10%	1%	10%	1%	10%	Rec.@1	Rec.@5	Wst.@1	Wst.@5
Decentralized	GLoRIA	82.34	82.89	77.90	88.75	71.07	72.13	17.15	52.50	15.19	48.73
FedAvg	GLoRIA	83.16	83.28	77.50	89.00	71.37	72.38	29.90	73.80	27.78	69.46
FedAID	GLoRIA	83.39	83.51	78.50	89.25	72.43	73.50	30.94	73.89	27.86	69.53
Centralized	GLoRIA	84.01	84.74	82.25	91.75	73.63	73.64	41.69	84.04	39.00	80.52
Decentralized	MGCA	81.90	82.71	77.80	87.55	62.77	70.20	15.21	50.44	13.37	45.39
FedAvg	MGCA	82.63	83.54	75.75	88.25	70.06	71.39	29.33	73.71	26.81	70.49
FedAID	MGCA	82.76	83.61	77.75	88.25	70.71	72.52	29.96	74.15	27.11	69.53
Centralized	MGCA	83.96	84.49	79.50	89.50	70.71	72.52	39.89	83.50	36.88	80.28

5.3 Main Result

Our method learns robust and enriched cross-modal alignment and has better transferability. Table 5.2 shows the image-text retrieval results. Here we utilize the ConVIRT as the backbone

pre-training method. Both average and worst-client accuracies of our method are higher than baseline’s, which means our model can not only capture more cross-modal alignment but optimize the performance on the worst client dataset, which verifies the robustness and fairness of our DRO-based strategy. Table 5.2 shows the results of the classification and segmentation downstream tasks. Our method beats other baseline strategies on each task and can be comparable to the centralized trained model, which acts as the upper bound. Therefore, our method has better transferability.

Previous single-modality methods cannot be adapted directly for multi-modal data. Table 5.2 shows the performance of adapted self-supervised federated learning methods which focus on single-modality. From the results, we observe that baselines have shown transferability on visual downstream tasks. However, in the multi-modal retrieval task, our method beats these baselines by a large margin, which indicates that previous single-modality methods cannot be easily adapted directly for multi-modal data. We conjecture this is because they have ignored modeling the cross-modal alignment. Furthermore, we think FedAvg is still a strong baseline compared to other adapted methods, as we observed in the experiments. That’s because FedAvg doesn’t hurt the ability to learn cross-modal alignment of backbone pre-training models by adding augmented losses.

Our method can be transferred to multiple multi-modal pre-training methods. Table 5.2 shows the downstream task performance of the MGCA and the GLoRIA backbone pre-training method when combined with our strategy. Our method has successfully upgraded MGCA and GLoRIA to adapt to the heterogeneous federated multi-modal pre-training scene, as shown in the significant improvement of the classification and segmentation downstream tasks.

5.4 Analysis experiment

In this section, we conduct analysis experiments using ConVIRT as backbone pre-training method. Table 3: Ablation results. We report the few-shot classification accuracy and the retrieval accuracy.

Alignment Module	Guidance	1% (cls.)		Chest imaG. (ret.)			
		Covid	RSNA	Rec.@1	Rec.@5	Wst.@1	Wst.@5
Simple-Average	L2	83.14	79.75	28.31	72.18	26.26	66.56
DRO learned	Contrastive	82.91	78.25	28.81	71.03	25.95	66.42
DRO learned	L2	83.21	80.50	29.49	26.99	73.03	67.65

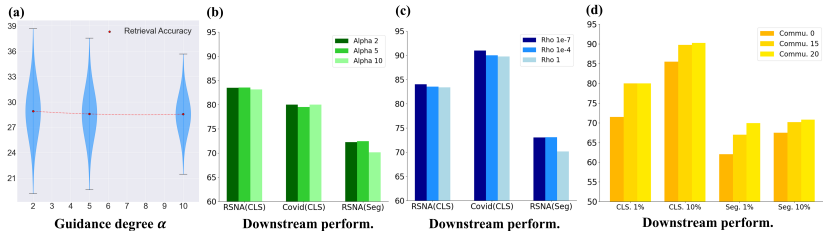


Figure 3: Analysis experiments on hyper-parameters. (a). The disparity-mean trade-off of cross-modal alignment adjusted by the guidance degree α . (b). Robustness of transferability on different α . (c). The effect of uncertainty radius ρ on downstream tasks. (d). Convergence capability.

Robust teacher align module is better than simply averaged one. To investigate the efficiency of the robust align module, we replace it with an align module that is simply averaged by local ones and pre-train a new model. As shown in table 5.4, the downstream performance of the replaced one is lower than the original one. This means the robust align module can enhance the ability to capture cross-modal alignments and learn transferable representation.

Strong regularization is better than weak regularization for guiding the updation. To investigate the effect of the guidance from the robust align module, we replace the L-2 regularization with contrastive loss as a weaker regularization and pre-train a new model. As shown in table 5.4, the weaker guidance leads to lower classification accuracy and retrieval accuracy in downstream tasks.

Guidance hyper-parameter adjusts the average and disparity of client performances. Fig. 3.a shows that higher guidance achieves smaller disparity while bringing less harm on average performance. We changed the hyperparameter α from 2 to 10, the disparity of the retrieval accuracy on test sets of different clients decreased significantly while there was only a slight loss on the averaged performance. On the other hand, Fig. 3.b shows that increasing α wouldn’t result in a penalty in the transferability of the pre-trained backbone, the downstream task performances are maintained at a high level as we enlarge the guidance. Detailed results can be seen in Table D.

Smaller radius of uncertain set brings higher generalization and transferability on downstream task. Fig. 3.c shows the downstream performance of models pre-trained with different radius of uncertainty set in the DRO process. As the ρ increases, the performance of fine-tuning-based downstream tasks shows an upward trend. Detailed results can be seen in Table C.

Convergence. We show the transferability of our models pre-trained with different communication turns in Fig. 3.d. As commun. turn reaches 20, the downstream performances tend to converge.

We have also conducted experiments to explore other properties of our proposed method. We have found that (1). Our method has successfully avoided the distortion caused by heterogeneous datasets during the local training. (2). Bringing more diverse clients for the federated pre-training is likely to improve the performance of the pre-trained model. (3). Our method is more generalizable on out-of-distribution multi-modal X-Ray datasets. Detailed results can be seen in Appendix C

6 Conclusion

Data limitation is a long-standing problem in the multi-modal learning domain. Despite federated learning can leveraging datasets from multiple sources while guaranteeing privacy issues, its performance would be damaged by data heterogeneity. Inspired by our empirical findings on the impact of heterogeneity on federated multi-modal learning, we propose the FedAID framework to multigate heterogeneity for federated medical vision-language pre-training. The efficiency of our method has been verified by comprehensive experiments. While introducing representation from other clients might bring larger improvement, we still consider the most privacy-preserved setting where representations are not transmissible. Further work could explore how to introduce data diversity while keeping local data private.

7 Acknowledgement

Zitao Shuai and Liyue Shen acknowledges support from U-M MIDAS PODS Grant and U-M MICDE Catalyst Grant, and computing resource support from NSF ACCESS Program. This work used NCSA Delta GPU through allocation CIS230133 and ELE230011 from the Advanced Cyberinfrastructure Coordination Ecosystem: Services & Support (ACCESS) program, which is supported by National Science Foundation grants 2138259, 2138286, 2138307, 2137603, and 2138296.

References

- Arora, S., Khandeparkar, H., Khodak, M., Plevrakis, O., and Saunshi, N. A theoretical analysis of contrastive unsupervised representation learning. *arXiv preprint arXiv:1902.09229*, 2019.
- Bae, S., Kyung, D., Ryu, J., Cho, E., Lee, G., Kweon, S., Oh, J., Ji, L., Chang, E. I., Kim, T., et al. Ehrxqa: A multi-modal question answering dataset for electronic health records with chest x-ray images. *arXiv preprint arXiv:2310.18652*, 2023.
- Bannur, S., Hyland, S., Liu, Q., Perez-Garcia, F., Ilse, M., Castro, D. C., Boecking, B., Sharma, H., Bouzid, K., Thieme, A., et al. Learning to exploit temporal structure for biomedical vision-language processing. In *Proceedings of the IEEE/CVF Conference on Computer Vision and Pattern Recognition*, pp. 15016–15027, 2023.
- Bao, H., Wang, W., Dong, L., Liu, Q., Mohammed, O. K., Aggarwal, K., Som, S., Piao, S., and Wei, F. Vlmo: Unified vision-language pre-training with mixture-of-modality-experts. *Advances in Neural Information Processing Systems*, 35:32897–32912, 2022.
- Bigolin Lanfredi, R., Zhang, M., Auffermann, W. F., Chan, J., Duong, P.-A. T., Srikumar, V., Drew, T., Schroeder, J. D., and Tasdizen, T. Reflax, a dataset of reports and eye-tracking data for localization of abnormalities in chest x-rays. *Scientific data*, 9(1):350, 2022.
- Blei, D. M., Ng, A. Y., and Jordan, M. I. Latent dirichlet allocation. *Journal of machine Learning research*, 3(Jan):993–1022, 2003.

- Capitani, G., Bolelli, F., Porrello, A., Calderara, S., and Ficarra, E. Clusterfix: A cluster-based debiasing approach without protected-group supervision. In *Proceedings of the IEEE/CVF Winter Conference on Applications of Computer Vision*, pp. 4870–4879, 2024.
- Chen, H., Zhang, Y., Krompass, D., Gu, J., and Tresp, V. Feddat: An approach for foundation model finetuning in multi-modal heterogeneous federated learning. *arXiv preprint arXiv:2308.12305*, 2023.
- Chen, J. and Zhang, A. Fedmsplit: Correlation-adaptive federated multi-task learning across multimodal split networks. In *Proceedings of the 28th ACM SIGKDD Conference on Knowledge Discovery and Data Mining*, pp. 87–96, 2022.
- Chen, L., Gan, Z., Cheng, Y., Li, L., Carin, L., and Liu, J. Graph optimal transport for cross-domain alignment. In *International Conference on Machine Learning*, pp. 1542–1553. PMLR, 2020.
- Chen, Z., Du, Y., Hu, J., Liu, Y., Li, G., Wan, X., and Chang, T.-H. Multi-modal masked autoencoders for medical vision-and-language pre-training. In *International Conference on Medical Image Computing and Computer-Assisted Intervention*, pp. 679–689. Springer, 2022.
- Collins, L., Hassani, H., Mokhtari, A., and Shakkottai, S. Exploiting shared representations for personalized federated learning. In *International conference on machine learning*, pp. 2089–2099. PMLR, 2021.
- Cotter, A., Jiang, H., Gupta, M., Wang, S., Narayan, T., You, S., and Sridharan, K. Optimization with non-differentiable constraints with applications to fairness, recall, churn, and other goals. *Journal of Machine Learning Research*, 20(172):1–59, 2019.
- Deng, Y., Kamani, M. M., and Mahdavi, M. Distributionally robust federated averaging. *Advances in neural information processing systems*, 33:15111–15122, 2020.
- Devlin, J., Chang, M.-W., Lee, K., and Toutanova, K. Bert: Pre-training of deep bidirectional transformers for language understanding. *arXiv preprint arXiv:1810.04805*, 2018.
- Diao, E., Ding, J., and Tarokh, V. Heterofl: Computation and communication efficient federated learning for heterogeneous clients. *arXiv preprint arXiv:2010.01264*, 2020.
- Dosovitskiy, A., Beyer, L., Kolesnikov, A., Weissenborn, D., Zhai, X., Unterthiner, T., Dehghani, M., Minderer, M., Heigold, G., Gelly, S., et al. An image is worth 16x16 words: Transformers for image recognition at scale. *arXiv preprint arXiv:2010.11929*, 2020.
- Duchi, J., Shalev-Shwartz, S., Singer, Y., and Chandra, T. Efficient projections onto the l_1 -ball for learning in high dimensions. In *Proceedings of the 25th international conference on Machine learning*, pp. 272–279, 2008.
- Ghosh, A., Hong, J., Yin, D., and Ramchandran, K. Robust federated learning in a heterogeneous environment. *arXiv preprint arXiv:1906.06629*, 2019.
- Han, P., Liu, Z., Liu, Z., and Xiong, C. Distributionally robust unsupervised dense retrieval training on web graphs. *arXiv preprint arXiv:2310.16605*, 2023.
- Huang, S.-C., Shen, L., Lungren, M. P., and Yeung, S. Gloria: A multimodal global-local representation learning framework for label-efficient medical image recognition. In *Proceedings of the IEEE/CVF International Conference on Computer Vision*, pp. 3942–3951, 2021a.
- Huang, W., Yi, M., Zhao, X., and Jiang, Z. Towards the generalization of contrastive self-supervised learning. *arXiv preprint arXiv:2111.00743*, 2021b.
- Huang, W., Ye, M., and Du, B. Learn from others and be yourself in heterogeneous federated learning. In *Proceedings of the IEEE/CVF Conference on Computer Vision and Pattern Recognition*, pp. 10143–10153, 2022.
- Jiang, M., Roth, H. R., Li, W., Yang, D., Zhao, C., Nath, V., Xu, D., Dou, Q., and Xu, Z. Fair federated medical image segmentation via client contribution estimation. In *Proceedings of the IEEE/CVF Conference on Computer Vision and Pattern Recognition*, pp. 16302–16311, 2023.

- Krishnan, R., Rajpurkar, P., and Topol, E. J. Self-supervised learning in medicine and healthcare. *Nature Biomedical Engineering*, 6(12):1346–1352, 2022.
- Ladbury, C., Amini, A., Govindarajan, A., Mambetsariev, I., Raz, D. J., Massarelli, E., Williams, T., Rodin, A., and Salgia, R. Integration of artificial intelligence in lung cancer: Rise of the machine. *Cell Reports Medicine*, 2023.
- Li, D. and Wang, J. Fedmd: Heterogenous federated learning via model distillation. *arXiv preprint arXiv:1910.03581*, 2019.
- Li, J., Selvaraju, R., Gotmare, A., Joty, S., Xiong, C., and Hoi, S. C. H. Align before fuse: Vision and language representation learning with momentum distillation. *Advances in neural information processing systems*, 34:9694–9705, 2021a.
- Li, J., Li, D., Xiong, C., and Hoi, S. Blip: Bootstrapping language-image pre-training for unified vision-language understanding and generation. In *International Conference on Machine Learning*, pp. 12888–12900. PMLR, 2022a.
- Li, J., Lyu, L., Iso, D., Chakrabarti, C., and Spranger, M. Mocosfl: enabling cross-client collaborative self-supervised learning. In *The Eleventh International Conference on Learning Representations*, 2022b.
- Li, Q., He, B., and Song, D. Model-contrastive federated learning. In *Proceedings of the IEEE/CVF conference on computer vision and pattern recognition*, pp. 10713–10722, 2021b.
- Li, Q., Diao, Y., Chen, Q., and He, B. Federated learning on non-iid data silos: An experimental study. In *2022 IEEE 38th International Conference on Data Engineering (ICDE)*, pp. 965–978. IEEE, 2022c.
- Liu, J., Shen, Z., Cui, P., Zhou, L., Kuang, K., and Li, B. Distributionally robust learning with stable adversarial training. *IEEE Transactions on Knowledge and Data Engineering*, 2022.
- Lu, S., Liu, Z., Liu, T., and Zhou, W. Scaling-up medical vision-and-language representation learning with federated learning. *Engineering Applications of Artificial Intelligence*, 126:107037, 2023a.
- Lu, W., Yu, H., Wang, J., Teney, D., Wang, H., Chen, Y., Yang, Q., Xie, X., and Ji, X. Zoopfl: Exploring black-box foundation models for personalized federated learning. *arXiv preprint arXiv:2310.05143*, 2023b.
- McMahan, B., Moore, E., Ramage, D., Hampson, S., and y Arcas, B. A. Communication-efficient learning of deep networks from decentralized data. In *Artificial intelligence and statistics*, pp. 1273–1282. PMLR, 2017.
- Namkoong, H. and Duchi, J. C. Stochastic gradient methods for distributionally robust optimization with f-divergences. *Advances in neural information processing systems*, 29, 2016.
- Oquab, M., Darcet, T., Moutakanni, T., Vo, H., Szafraniec, M., Khalidov, V., Fernandez, P., Haziza, D., Massa, F., El-Nouby, A., et al. Dinov2: Learning robust visual features without supervision. *arXiv preprint arXiv:2304.07193*, 2023.
- Radford, A., Kim, J. W., Hallacy, C., Ramesh, A., Goh, G., Agarwal, S., Sastry, G., Askell, A., Mishkin, P., Clark, J., et al. Learning transferable visual models from natural language supervision. In *International conference on machine learning*, pp. 8748–8763. PMLR, 2021.
- Saab, K., Hooper, S., Chen, M., Zhang, M., Rubin, D., and Ré, C. Reducing reliance on spurious features in medical image classification with spatial specificity. In *Machine Learning for Healthcare Conference*, pp. 760–784. PMLR, 2022.
- Shih, G., Wu, C. C., Halabi, S. S., Kohli, M. D., Prevedello, L. M., Cook, T. S., Sharma, A., Amorosa, J. K., Arteaga, V., Galperin-Aizenberg, M., et al. Augmenting the national institutes of health chest radiograph dataset with expert annotations of possible pneumonia. *Radiology: Artificial Intelligence*, 1(1):e180041, 2019.
- Su, S., Yang, M., Li, B., and Xue, X. Cross-domain federated adaptive prompt tuning for clip. *arXiv preprint arXiv:2211.07864*, 2022.

- Wang, F., Zhou, Y., Wang, S., Vardhanabhuti, V., and Yu, L. Multi-granularity cross-modal alignment for generalized medical visual representation learning. *Advances in Neural Information Processing Systems*, 35:33536–33549, 2022.
- Wang, L., Lin, Z. Q., and Wong, A. Covid-net: A tailored deep convolutional neural network design for detection of covid-19 cases from chest x-ray images. *Scientific reports*, 10(1):19549, 2020.
- Wu, J. T., Agu, N. N., Lourentzou, I., Sharma, A., Paguio, J. A., Yao, J. S., Dee, E. C., Mitchell, W., Kashyap, S., Giovannini, A., et al. Chest imagenome dataset (version 1.0. 0). *PhysioNet*, 5:18, 2021.
- Yan, R., Qu, L., Wei, Q., Huang, S.-C., Shen, L., Rubin, D., Xing, L., and Zhou, Y. Label-efficient self-supervised federated learning for tackling data heterogeneity in medical imaging. *IEEE Transactions on Medical Imaging*, 2023.
- Yang, J., Duan, J., Tran, S., Xu, Y., Chanda, S., Chen, L., Zeng, B., Chilimbi, T., and Huang, J. Vision-language pre-training with triple contrastive learning. In *Proceedings of the IEEE/CVF Conference on Computer Vision and Pattern Recognition*, pp. 15671–15680, 2022.
- Ye, M., Fang, X., Du, B., Yuen, P. C., and Tao, D. Heterogeneous federated learning: State-of-the-art and research challenges. *ACM Computing Surveys*, 56(3):1–44, 2023.
- Yu, Q., Liu, Y., Wang, Y., Xu, K., and Liu, J. Multimodal federated learning via contrastive representation ensemble. *arXiv preprint arXiv:2302.08888*, 2023.
- Zhang, F., Kuang, K., Chen, L., You, Z., Shen, T., Xiao, J., Zhang, Y., Wu, C., Wu, F., Zhuang, Y., et al. Federated unsupervised representation learning. *Frontiers of Information Technology & Electronic Engineering*, 24(8):1181–1193, 2023a.
- Zhang, F., Shuai, Z., Kuang, K., Wu, F., Zhuang, Y., and Xiao, J. Unified fair federated learning for digital healthcare. *Patterns*, 2023b.
- Zhang, G., Wei, S., Pang, H., and Zhao, Y. Heterogeneous feature fusion and cross-modal alignment for composed image retrieval. In *Proceedings of the 29th ACM International Conference on Multimedia*, pp. 5353–5362, 2021.
- Zhang, Y., Gao, H., Pei, J., and Huang, H. Robust self-supervised structural graph neural network for social network prediction. In *Proceedings of the ACM Web Conference 2022*, pp. 1352–1361, 2022a.
- Zhang, Y., Jiang, H., Miura, Y., Manning, C. D., and Langlotz, C. P. Contrastive learning of medical visual representations from paired images and text. In *Machine Learning for Healthcare Conference*, pp. 2–25. PMLR, 2022b.
- Zhou, K. and Wang, X. E. Fedvln: Privacy-preserving federated vision-and-language navigation. In *European Conference on Computer Vision*, pp. 682–699. Springer, 2022.
- Zhuang, W., Wen, Y., and Zhang, S. Divergence-aware federated self-supervised learning. *arXiv preprint arXiv:2204.04385*, 2022.

A Empirical Finding

In this section, we will demonstrate our key empirical findings for federated multi-modal pre-training under heterogeneous client datasets, which actually motivates us to propose our FedAID. We conduct experiments on the image-text retrieval task, which reflects the ability to capture vision-language alignments. We utilize the ConVIRT backbone strategy and consider the performance of the centralized pre-trained model (Global), the server model pre-trained in FedAvg(FedAvg), and the average performance of decentralized pre-trained local models (Local.avg.).

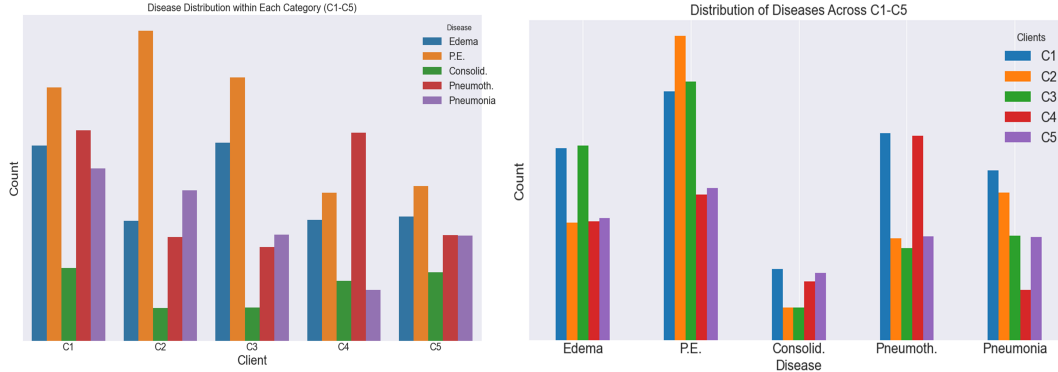


Figure 4: The disease distribution of the divided 5 subgroups, they are highly heterogeneous.

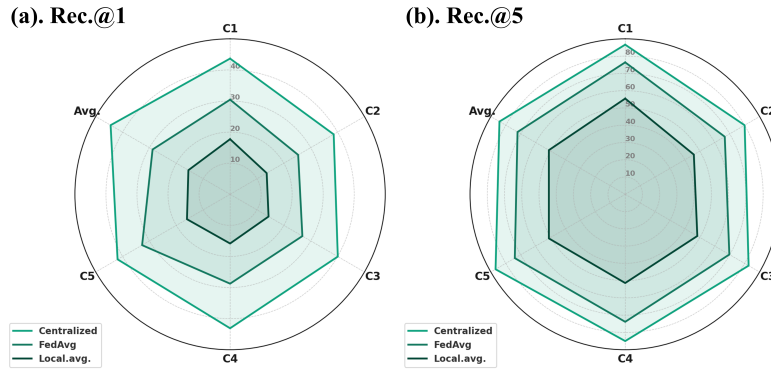


Figure 5: The comparison of retrieval acc. on each client denoted as $\{C_i\}_{i=1}^5$, of centralized, FedAvg, and averaged acc. of decentralized pre-trained models.

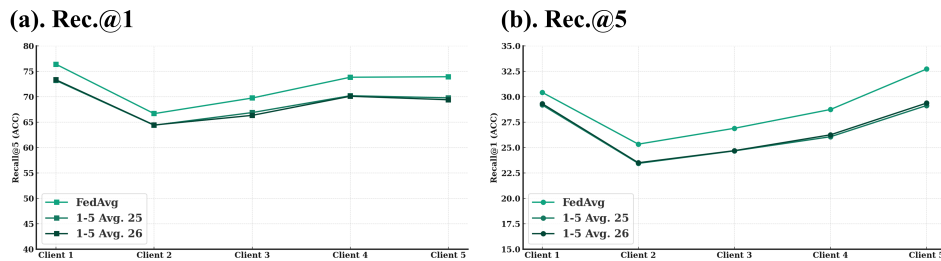


Figure 6: The performance of the server model after 25 com. turns and the averaged performance of corresponding client models after 25 and 26 com. turns, on each client denoted as $\{Client_i\}_{i=1}^5$.

FedAvg can aggregate semantics from local clients, but the performance would be damaged by data heterogeneity. Fig. 5 shows retrieval accuracies of the strategies we have considered, where the FedAvg pre-trained model achieves higher accuracies than those of decentralized ones with a large

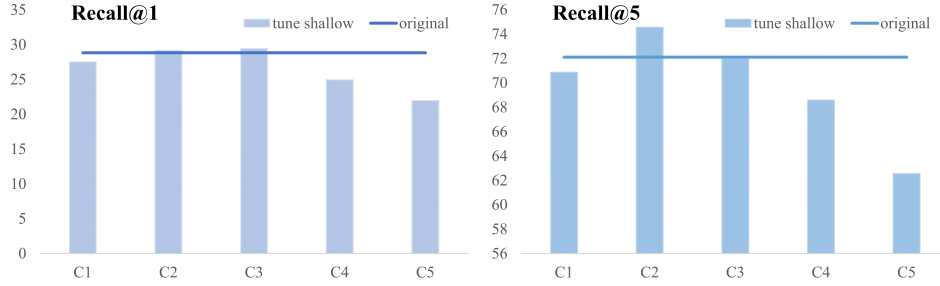


Figure 7: The averaged acc. on the test set of each client. We show the performance of FedAvg pre-trained baseline and its retrained models on different client datasets shown as $\{C_i\}_{i=1}^5$.

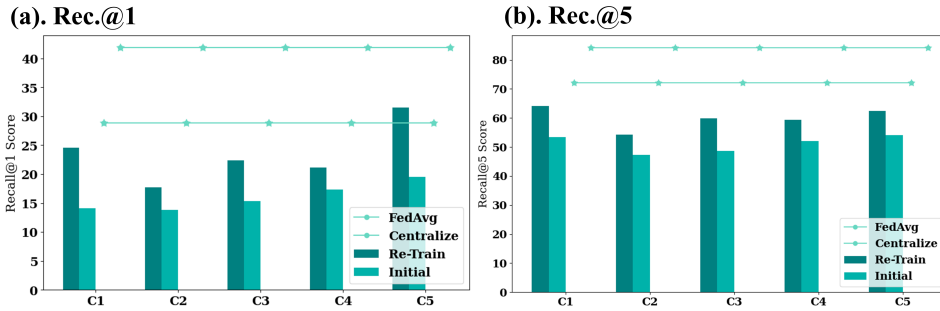


Figure 8: The averaged acc. on each client. We show the acc. of centralized and FedAvg pre-trained baselines, and de-centralized pre-trained models shown as $\{C_i\}_{i=1}^5$ retrained on the union of training splits of client datasets.

margin. However, the centralized pre-trained model acts as an upper bound and there still exists a great space for improvement for FedAvg. Table D in the appendix shows the detailed result. Further, we examine if updating the aggregated server model in FedAvg would result in distortion in the learned representation space.

Retraining the server model on local datasets would distort its feature encoders. Fig. 6 demonstrates the effect of distortion by fitting local cross-modal alignments of the corresponding client datasets. We consider a set of models that finished the 25th local iteration and their corresponding aggregated server model. While the average accuracy of local models is less than their aggregated model, the average performance of models re-trained on local clients starting from the aggregated model degrades a lot. Table D in the appendix shows the detailed results.

Diverse information is aggregated in shallow layers that mainly extract feature semantics. We re-train the first 4 shallow layers of the aggregated server model on local clients’ datasets for 500 iteration steps. As shown in Fig. 7, the performance of retrained models decreases a lot, which means shallow layers that extract feature semantics are distorted by heterogeneous local datasets. Table D in the appendix shows the detailed results.

De-centralized pre-trained deep layers that act as the align module is harmful for extracting diverse semantics. We re-train the first 4 shallow layers of the decentralized pre-trained model on the union of client datasets for 500 steps. Although the performance has successfully increased, there is still a large gap between that of the FedAvg pre-trained baselines and them as shown in Fig. 8. Therefore, the frozen deep layers prevent the model from learning more diverse semantics from the scaled dataset. Table D in the appendix shows the detailed results.

Overall, from the empirical findings, we conclude that federated multimodal pre-training is sensitive to the data heterogeneity which results in learning distorted cross-modal alignment. Simply averaging the local model weights does not solve this issue essentially. Thus, we are motivated to propose our FedAID.

B Experiment Details

B.1 Pre-training setup

Following Wang et al. (2022) we utilize the MIMIC-CXR Bigolin Lanfredi et al. (2022) dataset for multi-modal pre-training. This dataset is widely used in the medical multi-modal learning domain, with 227,835 image-text pairs from 65,379 patients. Some related works also have imported additional features to image-text pairs to augment the data. However, we only use the image-text pairs for pre-training to make the results more generalizable. The MIMIC-CXR dataset is open access, it can be obtained through MIMIC-CXR Access.

During the pre-training, local clients only have access to their highly heterogeneous datasets. To construct the heterogeneous client datasets, following Yan et al. (2023) we employ the Latent Dirichlet Allocation (LDA) Blei et al. (2003) to divide the MIMIC-CXR dataset into 5 partitions based on a selected sensitive attribute. For implementation, we import the corresponding attribute information of given image-text pairs from the Chest-Imagenone dataset Wu et al. (2021) and divide local datasets based on disease category. The disease category is a multi-label binary attribute and is transformed into a multi-class label. That’s because the words in the clinical report are highly related to the disease category as illustrated in Fig 9. We set the heterogeneity degree in the LDA algorithm to be 1 and the subgroups of the MIMIC-CXR that are used as local datasets are summarized in Table B.1.

Specifically, we select 5 commonly considered diseases Bannur et al. (2023): ‘Edema’, ‘Pleural Effusion’, ‘Consolidation’, ‘Pneumothorax’, and ‘Pneumonia’. We set the non-NaN value to 1 and then set NaN value to 0 to construct a 5-way binary multi-label. Then we get 2^5 -category multi-class label, and we run LDA on it. The distribution of the disease of the client dataset is summarized in Table B.1.

Report Sample 1:	
Previous mild pulmonary edema and possible concurrent pneumonia has all cleared. Heart is top-normal size, improved, and pleural effusions have resolved. Right hilar vessels are still enlarged, perhaps due to pulmonary arterial hypertension. Lateral view shows atherosclerotic coronary calcification in the left circumflex.	Label: Edema Pneumonia Pleural Effusions
Report Sample 2:	
Allowing for differences in technique and projection, there has been little interval change in the appearance of the chest since the previous radiograph, with no new focal areas of consolidation to suggest the presence of pneumonia . Multifocal linear areas of scarring appear unchanged, previously attributed to sarcoidosis. Band-like opacity at periphery of left lung base has slightly worsened and is attributed to localize atelectasis.	Label: Pneumonia

Figure 9: Illustration of the strong connection between latent variable and the text modality.

We divide the MIMIC-CXR into 5 heterogeneous subgroups to construct 5 client datasets. Each divided dataset consists of train splits and test splits based on the notation of the MIMIC-CXR. We use $4 \times A40$ for pre-training and set the batch size to 388. We set the learning rate to 2×10^{-5} , the number of communications to 25. We set the uncertainty radius $\rho = 1$, hyper-parameter $\alpha = 1, \beta = 2$ in the main experiments. For each communication, we randomly sample 50 batches of data from the client datasets.

B.2 Downstream tasks

We conduct Few-shot classification, Medical image segmentation, and Image Retrieval downstream tasks to evaluate the generalization ability of the pre-trained model.

Few-shot classification. To verify the efficiency of the pre-trained model on the general medical image task, we test their performance on multiple image classification benchmarks: (1) RSNA Pneumonia Detection (RSNA) Shih et al. (2019), the task is to predict if the image reflects a pneumonia-positive phenomenon. (2) Covidx Wang et al. (2020), which has three categories that COVID-19, non-COVID pneumonia and normal. We fine-tune our pre-trained model with an additional linear layer on 1%, 10% percentage of the training dataset of downstream tasks, and evaluate the image classification accuracy. For evaluation, we report the classification accuracy of the models on them.

Medical image segmentation. To investigate the transfer ability of our model on fine-grained tasks, we conduct experiments on medical image segmentation on the RSNA Wang et al. (2020) benchmark.

Table 4: The distribution of the sensitive attribute age-decile. From this table, we can verify that the local datasets are highly heterogeneous.

Edema	P. E.	Consolid.	Pneumothorax	Pneumonia	C1	C2	C3	C4	C5
					8251	52931	23153	16054	2983
Yes					367	130	4362	1993	2671
	Yes				67	11425	5825	778	655
Yes	Yes				945	1693	3472	2640	1607
		Yes			1641	261	599	791	1057
Yes		Yes			420	61	198	245	14
	Yes	Yes			253	50	18	805	913
Yes	Yes	Yes			434	95	27	303	153
			Yes		476	2504	128	8791	1097
Yes			Yes		827	284	559	603	156
	Yes		Yes		4366	1866	3507	2815	1140
Yes	Yes		Yes		5965	217	510	109	921
		Yes	Yes		123	80	444	111	84
Yes		Yes	Yes		48	9	101	4	269
	Yes	Yes	Yes		807	121	3	922	670
Yes	Yes	Yes	Yes		723	818	42	246	69
				Yes	7447	3656	1505	246	1395
Yes				Yes	278	927	719	1547	453
	Yes			Yes	98	970	1111	639	1145
Yes	Yes			Yes	2777	3019	2276	105	466
		Yes		Yes	10	323	120	227	760
Yes		Yes		Yes	31	57	153	28	9
	Yes	Yes		Yes	30	16	238	148	91
Yes	Yes	Yes		Yes	92	74	9	101	36
			Yes	Yes	208	286	48	15	33
Yes			Yes	Yes	70	214	248	1	90
	Yes		Yes	Yes	164	76	39	126	872
Yes	Yes		Yes	Yes	133	251	417	155	1224
		Yes	Yes	Yes	71	6	15	8	8
Yes		Yes	Yes	Yes	2	56	42	3	20
	Yes	Yes	Yes	Yes	156	18	11	44	279
Yes	Yes	Yes	Yes	Yes	38	156	201	38	183

We follow Wang et al. (2022) to convert object detection ground truths of RSNA into masks for semantic segmentation. Similar to Huang et al. (2021a), we construct a U-Net framework using a decoder and our pre-trained image encoder. During the fine-tuning, we freeze the encoder and fine-tune the decoder using 1%, 10% of the training data of the downstream dataset, and then use the Dice score to evaluate the performance of our model.

Image retrieval. To verify if the pre-trained models have learned the semantics and alignment relationships between the image and text contained in the pre-training dataset, we conduct the image retrieval downstream task. Specifically, we utilize the validation splits of the local clients to test the image retrieval performance of the aggregated models. For a text from a given batch of input image-text pairs, we calculate the similarities between this text and images in this batch. Then we sort these similarities and select the top-1 and top-5 images from them. If the corresponding image of the text is contained in the selected set, then the image is retrieved correctly. Here we utilize the top-1 recall accuracy and top-5 recall accuracy to evaluate the pre-trained models.

Out-of-Distribution testing benchmark. We adapt the EHRXQA Bae et al. (2023) VQA dataset for evaluation. This dataset is built on the meta-data notation of MIMIC-CXR Bigolin Lanfredi et al. (2022) and ChestImaGenome Wu et al. (2021). We merge the question and answer sentences as the text input and use the corresponding image to construct the image-text pairs for the multi-modal retrieval task. Other settings are the same as the ordinary image retrieval task.

B.3 Backbones and Baselines

We focus on enabling medical vision-language pre-training (VLP) methods to be applied to heterogeneous federated learning scenes and have considered the generalization ability of FedAID on different backbone VLP methods. Since federated heterogeneous VLP is a new topic, we adopt existing medical VLP baselines to federated strategies Lu et al. (2023a). Specifically, we consider adopting contrastive

learning based methods: simple language-image contrastive alignment (ConVIRT) Zhang et al. (2022b); Radford et al. (2021), global-local language-image contrastive alignment (GLoRIA) Huang et al. (2021a), and Multi-Granularity Cross-modal Alignment (MGCA) Wang et al. (2022). Since the federated multi-modal per-training is a novel setting, we adapted FedMAE Yan et al. (2023), FedEMA Zhuang et al. (2022), FedMOON Li et al. (2021b) for comparison. These are self-supervised learning methods in the federated learning domain which also focus on tackling the data heterogeneity. For basic federated learning baselines, we consider simple averaging (FedAvg) McMahan et al. (2017); Lu et al. (2023a), decentralized training (Local), and centralized training (Global). For fair comparisons, we combine each federated learning strategy with different medical VLP methods. For baselines pre-trained in Local strategy, we report the averaged performance of the local models.

For fair comparisons, we implement the method with the same backbones as our method. We utilize a ViT-Base model as our vision encoder and utilize the Bert-Base as our text encoder. We pre-process the input image following Wang et al. (2022) to resize the radiology graph to the size of 224×224 to match the vision encoder.

Table 5: Descriptive Statistics of the subgroups.

Disease	Client 1	Client 2	Client 3	Client 4	Client 5
Edema	13150	8061	13336	8121	8341
Pleural Effusion.	17048	20865	17706	9974	10424
Consolidation	4879	2201	2221	4024	4615
Pneumothorax	14177	6962	6315	13991	7115
Pneumonia	11605	10105	7152	3431	7064

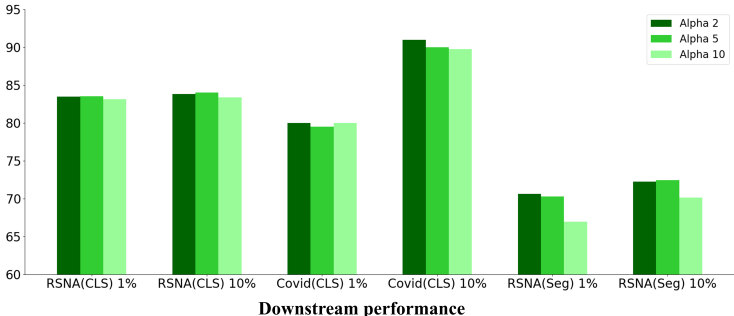


Figure 10: Role of guidance degree α . Increasing α results in at most small penalty in the transferability.

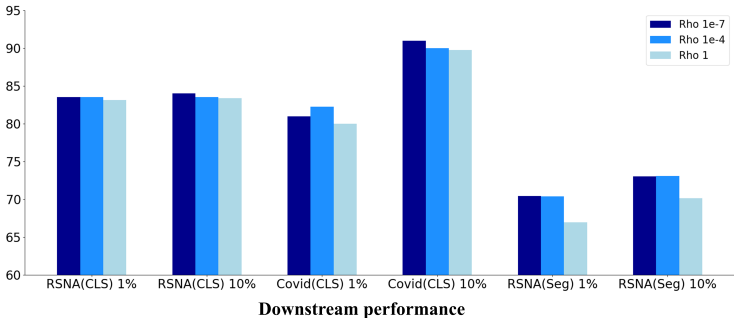


Figure 11: Role of the uncertainty radius ρ . A small radius of ρ brings higher generalization and transferability on downstream tasks.

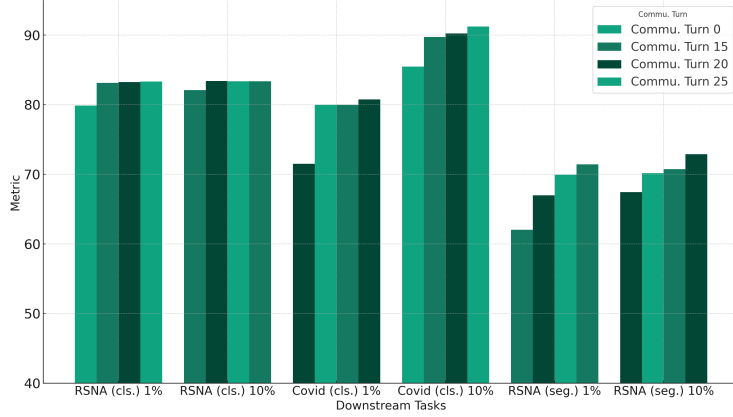


Figure 12: Robustness & convergence on the number of com. turns.

Table 6: Distortion of local training of FedAvg method. We show the performance gap between the server and local retrained models. We employ the decrease in the similarity of the image embedding and text embedding to be an indicator of distortion.

FedAvg	Test on C1	Test on C2	Test on C3	Test on C4	Test on C5
Retrain On C1	0.092	0.078	0.08	0.073	0.082
Retrain On C2	0.054	0.049	0.046	0.047	0.048
Retrain On C3	0.069	0.072	0.07	0.066	0.067
Retrain On C4	0.092	0.09	0.084	0.093	0.088
Retrain On C5	0.073	0.08	0.07	0.068	0.087
Avg	0.076	0.0738	0.07	0.0694	0.0744

Table 7: Detailed results on the analysis experiments of the role of hyper-parameter α .

ρ	RSNA (cls.)		Covid (cls.)		RSNA (seg.)	
	1%	10%	1%	10%	1%	10%
$\rho = 1e - 7$	83.51	84.04	81.00	91.00	70.44	73.05
$\rho = 1e - 4$	83.51	83.54	82.25	90.00	70.39	73.11
$\rho = 1$	83.16	83.41	80.00	89.75	66.98	70.18

Table 8: Ablation experiment results on the zero-shot generalization ability of our method on the real-world dataset.

Strategy	O.O.D		In domain		In domain Wst.	
	Rec.@1	Rec.@5	Rec.@1	Rec.@5	Rec.@1	Rec.@5
FedMAE	12.93	63.72	5.05	23.91	4.34	20.86
FedEMA	15.19	66.94	24.01	67.05	21.85	62.44
FedAvg	15.3	66.62	28.83	72.12	25.34	66.68
FedAID (Ours)	15.43	67.29	29.49	73.03	26.99	67.65

Table 9: Distortion of local training of ours method. We show the performance gap between the server and local retrained models. We employ the decrease in the similarity of the image embedding and text embedding to be an indicator of distortion.

Ours	Test on C1	Test on C2	Test on C3	Test on C4	Test on C5
Retrain On C1	0.025	0.023	0.017	0.034	0.01
Retrain On C2	0.046	0.05	0.043	0.057	0.063
Retrain On C3	0.05	0.052	0.044	0.055	0.036
Retrain On C4	0.062	0.043	0.038	0.041	0.033
Retrain On C5	0.071	0.058	0.048	0.066	0.053
Avg	0.0508	0.0452	0.038	0.0506	0.039

C Additional Analysis Experiment

Our method has successfully avoided the distortion caused by heterogeneous datasets during the local training. Empirically, we demonstrate the effectiveness of this guidance-based local training strategy. Specifically, we retrain the model on each local dataset with the same backbone methods and setting and conduct the study on the change of similarity between embeddings of paired image and text. We show the performance gap between the server and local retrained models. The reduced similarity of the image embedding and text embedding from paired data can be regarded as an indicator of "distortion" of cross-modal alignment. As reported in Table 6 and Table 9, we observe that the average decrease on the similarity of image and text embedding of our method is much smaller compared to FedAvg baseline.

Role of the number of clients that participated in the federated pre-training. We have conducted experiments on how the number of clients participating in the federated pre-training affects the performance of the learned model. As shown in the Table D, we have observed that bringing more diverse clients for the federated pre-training is likely to improve the performance of the pre-trained model.

Our method has better classification accuracies on unseen out-of-distribution multi-modal X-Ray datasets. The multi-modal retrieval accuracy in the unseen domain of our method beats the baseline by a large margin as shown in Table C, which verifies our method’s ability to learn generalizable cross-modal alignment. Meanwhile, our FedAID has higher in-domain averaged and worst-case acc.. Therefore, improvements in the in-domain performance of FedAID do not come at the cost of decreased out-of-domain performance.

Convergence check: As shown in Figure 12 the downstream performance of the pre-trained got promoted as we increased the number of comm. turns. After 20 communications, the performance turned out to be stable which verified the convergent ability of our method. Detailed results can be seen in Table D.

D Detailed Experiment Results

In addition to the experiment results shown in the above figures and tables, here we show the detailed points in Table 9, Table D, Table D, Table D, Table D, Table D, Table D, Table D and Table D.

Table 10: The comparison of retrieval acc. on each client denoted as $\{C_i\}_{i=1}^5$, of centralized, FedAvg, and averaged acc. of decentralized pre-trained models using the ConVIRT backbone. We report the local models of decentralized pre-training strategy as Decentralized_{*i*}.

Strategy	Recall@1 (ACC)					Recall@5 (ACC)						
	C1	C2	C3	C4	C5	Avg.	C1	C2	C3	C4	C5	Avg.
Centralized	43.65	38.55	40.08	43.10	41.86	44.45	86.63	79.98	82.65	84.99	86.83	84.22
FedAvg	30.43	25.34	26.90	28.75	32.73	28.83	76.39	66.68	69.75	73.84	73.94	72.12
Decentralized ₁	17.68	14.71	15.37	18.18	14.14	16.01	56.99	49.56	51.29	54.55	55.10	53.50
Decentralized ₂	15.33	11.62	13.85	14.96	13.83	13.92	54.84	41.93	46.20	47.90	45.62	47.30
Decentralized ₃	17.41	13.08	14.12	15.07	15.39	15.01	50.40	44.21	46.37	49.72	52.53	48.65
Decentralized ₄	16.54	14.34	14.08	15.36	17.35	15.53	57.02	45.72	47.45	52.38	57.63	52.04
Decentralized ₅	21.68	14.34	14.20	15.56	19.50	17.06	57.89	48.43	50.18	52.36	61.66	54.10
Local.avg.	17.73	13.62	14.32	15.83	16.04	15.51	55.43	45.97	48.30	51.38	51.12	51.12

E Problem Position

The federated vision-language pre-training is a more practical and general task compared to related works. Table D lists the most similar settings in previous works, and the difference between our task and theirs. Our federated multi-modal pre-training focuses on learning generalizable vision-language models which can be transferred to various downstream tasks, with paired unlabeled multi-modal data, in a fully decentralized way that can guarantee the data privacy required by clinical applications. We tackle the data heterogeneity problem in local training, which is a vital concern in federated

Table 11: The performance of the server model after 25 commu. turns and the averaged performance of corresponding local models after 25 and 26 commu. turns, on each client denoted as $\{C_i\}_{i=1}^5$. We utilize the ConVIRT as the backbone. We report the models after local update on client datasets of FedAvg pre-training strategy as Local $_i$.

Strategy	com. turn	Recall@1 (ACC)					Recall@5 (ACC)				
		C1	C2	C3	C4	C5	C1	C2	C3	C4	C5
FedAvg	25	30.43	25.34	26.90	28.75	32.73	76.39	66.68	69.75	73.84	73.94
Local ₀	25	31.75	23.37	25.96	26.21	33.71	73.44	64.14	67.15	71.38	71.79
Local ₁	25	27.72	22.52	23.77	25.06	27.70	73.45	63.08	64.57	69.15	68.58
Local ₂	25	28.55	24.37	24.30	27.26	28.93	73.26	64.94	67.52	70.28	71.75
Local ₃	25	30.63	22.62	23.90	25.36	26.42	72.57	64.02	66.26	68.92	67.62
Local ₄	25	27.31	24.37	25.47	26.47	28.93	73.26	65.83	68.95	71.23	69.21
1-5 Avg.	25	29.19↓	23.45↓	24.68↓	26.07↓	29.14↓	73.20↓	64.40↓	66.89↓	70.20↓	69.79↓
Local ₀	26	29.91	23.18	25.24	26.66	33.05	73.44	64.14	67.15	71.38	71.79
Local ₁	26	28.7	23.05	23.95	25.91	27.37	74.48	63.37	64.12	69.69	67.93
Local ₂	26	30.9	23.85	25.42	27.67	29.89	72.40	65.57	67.42	71.56	71.12
Local ₃	26	30.11	22.66	23.41	24.45	27.05	73.09	63.48	65.32	67.48	67.31
Local ₄	26	26.96	24.81	25.47	26.6	29.55	73.61	66.03	69.17	71.19	69.54
1-5 Avg.	26	29.32↓	23.51↓	24.70↓	26.26↓	29.38↓	73.33↓	64.44↓	66.34↓	70.10↓	69.41↓

Table 12: Robustness check on communication turns.

Com.	RSNA (cls.)		Covid (cls.)		RSNA (seg.)		Chest imaG. (ret.)			
	1%	10%	1%	10%	1%	10%	Rec.@1	Rec.@5	Wst.@1	Wst.@5
commu.=0	79.89	82.11	71.50	85.50	62.03	67.46	3.27	16.44	2.53	13.54
commu.=15	83.16	83.41	80.00	89.75	66.98	70.18	28.56	71.83	2595	67.21
commu.=20	83.26	83.39	80.00	90.25	69.93	70.76	29.69	72.09	26.75	67.52
commu.=25	83.34	83.39	80.75	91.25	71.42	72.89	29.80	72.59	27.48	68.64

Table 13: Detailed results on the analysis experiments of the role of hyper-parameter α .

Hyper. Alpha	RSNA (cls.)		Covid (cls.)		RSNA (seg.)		Chest imaG. (ret.)		
	1%	10%	1%	10%	1%	10%	Recall Acc.	Worst Acc.	Disparity
$\alpha = 2$	83.49	83.83	79.99	91.00	70.67	72.27	3.25	28.91	25.95
$\alpha = 5$	83.51	84.01	79.50	90.00	70.31	72.44	2.99	28.58	26.12
$\alpha = 10$	83.16	83.41	80.00	89.75	66.98	70.18	2.37	28.56	26.17

Table 14: Detailed results on the analysis experiments of the effect of the number of participated clients.

Num. Client	RSNA (cls.)		Covid (cls.)		RSNA (seg.)		Chest imaG. (ret.)			
	1%	10%	1%	10%	1%	10%	Rec@1 Acc.	Wst@1 Acc.	Rec@5 Acc.	Wst@5 Acc.
n=2	82.11	83.06	77.25	88.5	62.73	71.17	22.27	62.2	18.7	56.23
n=5	83.21	83.54	80.5	90	71.51	74.08	29.49	73.03	26.99	67.65

Table 15: The accuracy of the test set of each client. We show the performance of FedAvg pre-trained baseline and its retrained models on different client datasets. We report the models after local update on client datasets of FedAvg pre-training strategy as Local $_i$.

position	model	com.	Recall@1 (ACC)						Recall@5 (ACC)					
			C0	C1	C2	C3	C4	Avg.	C0	C1	C2	C3	C4	Avg.
-	server	25	30.43	25.34	26.90	28.75	32.73	28.83	76.39	66.68	69.75	73.84	73.94	72.12
-	server	50	32.29	26.03	26.99	27.06	30.23	28.52↓	77.60	67.86	69.43	72.06	71.74	71.74↓
→ shallow	Local ₀	25	30.35	24.95	25.32	28.44	28.62	27.54↓	73.78	67.22	68.44	71.95	73.01	70.88↓
→ shallow	Local ₁	25	34.25	26.4	27.27	29.66	30.20	29.44↑	78.30	69.75	72.33	75.07	77.42	74.57↑
→ shallow	Local ₂	25	33.68	26.39	27.27	29.66	30.20	29.44↑	77.25	67.37	70.67	74.21	70.51	72.02↑
→ shallow	Local ₃	25	27.65	18.94	19.30	25.61	24.87	24.95↓	72.40	64.19	64.82	70.47	71.13	68.60↓
→ shallow	Local ₄	25	26.19	18.94	19.30	22.74	22.66	21.97↓	69.27	56.76	58.94	63.35	64.50	62.56↓

Table 16: The accuracy of the model on each client. We show the acc. of centralized and FedAvg pre-trained baselines and de-centralized pre-trained models shown as Local_{*i*} retrained on the union of training splits of client datasets. We fine-tune shallow layers of the de-centralized pre-trained model with the union dataset.

strategy	model	Recall@1 (ACC)					Recall@5 (ACC)						
		C1	C2	C3	C4	C5	Avg.	C1	C2	C3	C4	C5	Avg.
Global	server	43.65	38.55	40.08	43.10	41.86	41.45	86.63	79.98	82.65	84.99	86.83	84.22
FedAvg	server	30.43	25.34	26.90	28.75	32.73	28.83	76.39	66.68	69.75	73.84	73.94	72.12
Decentralized	Local ₁	28.72	22.61	23.52	22.32	24.59	24.35	70.94	60.77	63.31	62.40	63.42	64.17
Decentralized	Local ₂	17.36	19.85	18.23	17.58	17.68	18.14	52.70	56.05	55.14	54.01	53.54	54.29
Decentralized	Local ₃	20.92	20.67	25.96	21.04	22.34	22.19	58.93	58.05	65.34	58.21	58.99	59.90
Decentralized	Local ₄	20.86	20.07	20.69	25.57	21.12	21.66	59.11	56.88	57.82	64.70	58.69	59.44
Decentralized	Local ₅	21.79	19.54	21.98	20.90	31.54	23.15	60.73	56.99	59.80	60.17	74.07	62.35
Decentralized	Local ₁	17.68	14.71	15.37	18.18	14.14	16.02	56.99	49.56	51.29	54.55	55.10	53.50
Decentralized	Local ₂	15.33	11.62	13.85	14.96	13.83	13.92	54.84	41.93	46.20	47.90	45.62	47.30
Decentralized	Local ₃	17.41	13.08	14.12	15.07	15.39	15.01	50.40	44.21	46.37	49.72	52.53	48.65
Decentralized	Local ₄	16.54	14.34	14.08	15.36	17.35	15.53	57.02	45.72	47.45	52.38	57.63	52.04
Decentralized	Local ₅	21.68	14.34	14.20	15.56	19.50	17.06	57.89	48.43	50.18	52.36	61.66	54.10

Table 17: Detailed ablation results.

Strategy	Recall@1 (ACC)					Recall@5 (ACC)						
	C1	C2	C3	C4	C5	Avg.	C1	C2	C3	C4	C5	Avg.
→avg.align.	30.11	26.26	26.63	30.30	28.27	28.31	74.65	66.56	70.23	73.62	75.83	72.18
→CL	30.80	25.95	26.27	29.24	31.78	28.81	74.13	66.42	68.09	71.65	74.86	71.03
ours	32.53	26.99	27.70	29.09	31.12	29.62	77.08	67.65	70.32	73.96	76.12	73.14

Table 18: Comparison between related tasks and our federated multi-modal pre-training task. We organize the related works based on our key areas of interest. (1). Heterogeneous clients. (2). Client-side pretraining. (3). Federated self-supervised learning (FSSL) to leverage unlabeled data. (4). multi-modal alignment. (5). Pre-train models that can be transferred to other downstream tasks. (6). No communication on public data or feature representations.

Task	hetero.	pretrain on client	FSSL.	align modalities	transfer.	no feat. commu.
Learn different client modalities Chen & Zhang (2022)	✓					✓
Augment server with local modality Yu et al. (2023)	✓		✓		✓	
FSSL. on unlabeled datasets Zhang et al. (2023a)		✓	✓			
FSSL with server fine-tune Yan et al. (2023)	✓	✓	✓			✓
Federated multi-modal pre-training	✓	✓	✓	✓	✓	✓

learning. During client-server communication, we avoid data transmission on features of local data to ensure data privacy.

F Detailed Problem Formulation

We aim at mitigating the data heterogeneity issues in federally pre-training medical vision-language models from heterogeneous private client datasets. In this section, we will formulate the set-up of the Federated Vision-Language Pre-training task, which aims to capture better cross-modal alignment by leveraging diverse semantics from local datasets. Then we will introduce our assumption on multi-modal pre-training data and heterogeneity. Please see Appendix F for the detailed preliminary.

Federated Vision-Language Pre-training (FedVLP). We aim to federally pre-train medical vision-language models. Specifically, given N clients $\{C_i\}_{i=1}^N$, FedVLP decentralizedly conducts vision-language representation learning across clients to learn local models, and aggregates them on a central server to obtain a more generalizable pre-trained model. Each client has a local yet private dataset $\{D_i\}_{i=1}^N$ that can't be easily shared due to privacy issues. During FedVLP, different from supervised federated learning, we focus on the transferability of the aggregated model.

Employing an alternative updating approach, federated pre-training also consists of multiple communication turns between clients and the server the same as conventional federated learning (FL) scenes.

For each turn t , client models $\{M_i^t\}_{i=1}^N$ completed local pre-training respectively and send model weights to server, then it receives and aggregates the weights to obtain server model M^t . M^t will be broadcast to clients for updating local models, and complete the main part of the communication turn. In some FL methods, additional local computation and information transmissions are conducted after clients have received the aggregated model, and they are counted as a part of the communication. The federated vision-language pre-training is a more practical and general task compared to related works. Table D in appendix lists the most similar settings in previous works, and their differences with ours.

Formulation of Multi-Model Pre-training Data and Heterogeneity. We consider the multimodal datasets including vision and language modalities X, Y , consisting of respective data samples $X = \{x_i\}_{i=1}^{n_1}, Y = \{y_i\}_{i=1}^{n_2}, n_1, n_2 \in N^+$. We assume there exists discrete multi-label latent variables U that embed semantics across two modalities such that $X = H_I(U), Y = H_T(U)$, where $H_I(\cdot), H_T(\cdot)$ are assumed transformations that is not explicit to know. For example, the disease category of a given X-ray radiology-report pair is a latent variable connecting these two modalities, which determines the pathology region of the radiology image and semantics in the diagnosis report. Thus, we assume each client has paired image-text data that are implicitly correlated through the same latent variables. Therefore, local client datasets could be written as $\mathcal{D} : \{D_i : (H_I(u), H_T(u)), u \sim P_i(U)\}_{i=0}^N$, where u can be thought as a latent class. Here, we assume the local datasets are heterogeneous, which means the distribution of latent variables $P_i(U)$ is different across clients.

We formulate two distributions $\mu_i \in P(X_i), \nu_i \in P(Y_i)$ following Chen et al. (2020) as $\mu_i = \sum_{j=1}^{n_i} a_j \delta_{T_x(u_j)}_{i,j}$ and $\nu_i = \sum_{j=1}^{n_i} b_j \delta_{T_y(u_j)}_{i,j}$, with δ_x as the Dirac function centered on x . The weight vectors $a_i = \{a_j\}_{j=1}^{n_i} \in \Delta_{n_i}$ and $b_i = \{b_j\}_{j=1}^{n_i} \in \Delta_{n_i}$ belong to the $(n-1)$ -dim simplex, where μ_i and ν_i are probability distributions. This formulation can also be applied to feature vectors or representations. For a given set of distributions $\{P_i\}_{i=1}^N$, we can form a new distribution $P^c = \sum_{i=1}^N w_i P_i, \mathbf{w} \in \Delta$ where Δ is a $(N-1)$ -dim simplex by weighted averaging the sample vectors.

Model Architectures. Following the VLP works Radford et al. (2021); Yang et al. (2022), we formulate the VLP using a dual-model structure, where the model for each modality consists of a feature encoder module $f(\cdot)$ that outputs feature vectors given the raw input, and a feature alignment module $g(\cdot)$ that projects feature vectors to aligned representations in the shared embedding space. We denote the feature vectors on the text side as l , the feature vectors on the image side as v , and the aligned representation as z_l, z_v respectively. During the distributionally robust optimization process, while we utilize the distribution of latent semantics to construct an uncertainty set for optimization, we take local alignment modules and the server-aggregated encoder as conditions.

Uncertainty set for Distributionally Robust Optimization (DRO). After the first stage in local training, the server aggregates the weights of local encoders to get f^* and sends it back to clients for learning a robust teacher alignment module g^* . We aim to optimize the alignment module on the worst-case distribution of an uncertainty set constructed by the local data distribution, which represents possible cases that the model would encounter. Specifically, a worst-case distribution is considered based on support distributions and the uncertain radius. We first consider the set of possible weighted combinations of support distributions and then enlarge the set by introducing an uncertain radius. We utilize distributions of latent semantics $P_i(U)$ of local clients as support distributions. Therefore, following the notation in F, the uncertainty set can be written as:

$$Q^c : \{D(Q||P^c) \leq \rho\}, P^c = \sum_{i=1}^N w_i P_i(U), w \in \Delta_{N-1} \quad (6)$$

where N is the number of clients, Δ is a $(N-1)$ -dim simplex, D is a discrepancy measure, and ρ is the uncertainty radius that measures the uncertainty degree of the unseen distributions and influences model's generalization ability.

G Analysis of Theoretical Insights

G.1 Theoretical Analysis on Remark 1

Here we provide a theoretical analysis on Remark 1 in Sec. 4.2. During the local training on client c , given the model parameter θ , we aim to show that optimizing $\min_{\theta} L_{\text{task}}(z_I^{c*}, z_T^{c*})$ can be reformulated as optimizing $\min_{\theta} (L_{\text{task}}(z_I^c, z_T^c) + \alpha (\|z_I^c - z_I^{c*}\|_2^2 + \|z_T^c - z_T^{c*}\|_2^2))$.

Since $L_{\text{task}}(x, y)$ is L -lipschitz, we have:

$$\|L_{\text{task}}(x_1, y_1) - L_{\text{task}}(x_2, y_2)\| \leq L(\|x_1 - x_2\| + \|y_1 - y_2\|). \quad (7)$$

Hence, we have:

$$\begin{aligned} L_{\text{task}}(z_I^{c*}, z_T^{c*}) &\leq \|L_{\text{task}}(z_I^{c*}, z_T^{c*}) - L_{\text{task}}(z_I^c, z_T^{c*})\| + \|L_{\text{task}}(z_I^c, z_T^{c*})\| \\ &\leq L(\|z_I^c - z_I^{c*}\| + \|z_T^{c*} - z_T^c\|) + \|L_{\text{task}}(z_I^c, z_T^c)\| \\ &= L\|z_I^c - z_I^{c*}\| + \|L_{\text{task}}(z_I^c, z_T^c)\| \\ &\leq L(\|z_I^c - z_I^{c*}\| + \|z_T^c - z_T^{c*}\|) + \|L_{\text{task}}(z_I^c, z_T^c)\| \\ &= L(\|z_I^c - z_I^{c*}\| + \|z_T^c - z_T^{c*}\|) + L_{\text{task}}(z_I^c, z_T^c) \end{aligned}$$

Therefore, $L(\|z_I^c - z_I^{c*}\| + \|z_T^c - z_T^{c*}\|) + \|L_{\text{task}}(z_I^c, z_T^c)\|$ can be an upper bound of the original learning object $L_{\text{task}}(z_I^{c*}, z_T^{c*})$. During local training, we add the L-2 regularization to guide the update of the local model. We also consider the contrastive loss to measure the distance between (z_T^c, z_I^c) and (z_T^{c*}, z_I^{c*}) in the ablation study. However, L-2 regularization brings better performance and matches our assumption.

G.2 Discussion on Cross-Modal Alignment

Here we illustrate why we model the cross-modal alignment as an alignment module that projects features of vision and language modalities to a shared representation space, and intends to minimize the distance between representations of the two modalities.

Following the notation in F, suppose we have features I, T of vision and language modalities, and the corresponding alignment module $g_I(\cdot), g_T(\cdot)$. Inspired by Huang et al. (2021b), suppose $g_I(\cdot), g_T(\cdot)$ are L -Lipschitz, we formulate the alignment degree of two domains as:

$$R_\epsilon = \mathbb{P} \left[u : \sup_{I=H_I(u), T=H_T(u)} \|g_I(I) - g_T(T)\| \geq \epsilon \right] \quad (8)$$

For a simple case following Huang et al. (2021b), the goal of the alignment module can be written as:

$$L_{\text{align}}(g_I, g_T) = \mathbb{E}_x \mathbb{E}_{I=H_I(u), T=H_T(u)} \|g_I(I) - g_T(T)\|^2 \quad (9)$$

Using the in Theorem 2 in Huang et al. (2021b) by replacing the encoder to our $g(\cdot)$, we have the following bound:

$$R_\epsilon^2 \leq \eta(\epsilon)^2 \cdot \mathbb{E}_u \mathbb{E}_{I=H_I(u), T=H_T(u) \in A(x)} \|g_I(I) - g_T(T)\|^2 = \eta(\epsilon)^2 \cdot L_{\text{align}}(g_I, g_T) \quad (10)$$

,where $\eta(\epsilon)$ is a infite function that corresponding to threshold ϵ .

Therefore, we model the cross-modal alignment as the alignment module that minimizes the distance between the representations of two modalities.

H Limitation

The design of the proposed FedAID approach has taken it into serious consideration to mitigate the potential negative societal impact.. For example, to tackle the data privacy issue, FedAID has avoided the transmission of any data or latent representations during all server-client communications, while only transferring model parameters and loss, thereby minimizing the risk of privacy leakage in federated learning as much as possible. However, our model may still be subject to privacy-related issues due to the communication of model parameters, which is a common problem faced by other federated learning methods as well. There are also research studies in this line to avoid privacy leakage from model parameters.

For fairness, our method aims at optimizing the performance of the worst-case client to promote model equity across different cohorts, which has shown great generalizable ability on unseen data. This approach ensures that the pre-trained model not only performs well and fairly on the data

from hospitals participating in the federated training but also demonstrates good performance on hospitals that did not participate in the training. Meanwhile we acknowledge that there may still exist limitations. Firstly, If we can resolve the trade-off between privacy protection and data representation communication, it may allow us to design more advanced algorithms to further enhance the performance of federated multimodal pre-training models.

Furthermore, in this work we mainly consider the multimodal medical datasets of X-Ray image-report due to the limitation of the public datasets. However, some rare diseases and more complicated modalities in various medical applications lack paired data, which] may bring other challenges for federated multimodal pretraining.